CoO_x/CeO_2 Nanocomposite Powders: Synthesis, Characterization, and Reactivity

Marta Maria Natile and Antonella Glisenti*

Dipartimento di Scienze Chimiche, Università di Padova, via Marzolo, 1-35131 Padova, Italy

Received July 30, 2004. Revised Manuscript Received March 18, 2005

CoO_x/CeO_2 nanocomposite materials with increasing Co/Ce atomic ratio were prepared by wet impregnation and characterized by means of X-ray photoelectron, diffuse reflectance infrared Fourier transform, and inductively coupled plasma atomic emission spectroscopic techniques, by BET and by thermal analysis. CoO is prevalent in the samples with lower cobalt content, whereas Co_3O_4 is the main presence at high Co/Ce atomic ratios. CeO_2 is slightly reduced: Ce(III) is evident at the interface supported/supporting oxide. X-ray diffraction and transmission electron microscopy allowed us to obtain interesting information concerning particle dimensions and growing morphology. The acidic/basic properties of the catalysts surfaces were investigated by studying the interaction of CoO_x/CeO_2 powder samples with pyridine and CO_2. New acidic/basic sites are evident on the surface of the nanocomposites; this is particularly evident in the samples with lower cobalt content. The interaction with methanol was also investigated. Methanol chemisorbs molecularly and dissociatively on the CoO_x/CeO_2 samples; dissociation is prevalent in the sample characterized by a lower content of cobalt oxide. The oxidation of methanol is evident at rather low temperatures. When water is added to methanol, the oxidation temperature decreases (373 K instead of 433 K) and the formation of carbon monoxide is not observed.

Introduction

A long time has elapsed from the first demonstration of fuel cells in 1839. The interest in fuel cells has increased significantly only in the past decades. In fact, environmental concerns about global warming and the need to reduce carbon dioxide emissions have prompted the search for improved energy conversion efficiency. In this respect, fuel cells, and solid oxide fuel cells (SOFCs) in particular, offer a very significant opportunity, thanks to their high efficiencies.[1,2] Several properties make SOFCs one of the most promising designs: the higher stability of the oxide materials and no problems with water management, flooding of the catalyst layer or slow oxygen reduction kinetics. Moreover, internal re-forming is possible in the SOFC over the anode catalyst.[3]

In this paper, we deal with cobalt oxide/ceria nanocomposite oxides. Our interest is in development of novel nanocomposite oxide-based systems to be used as advanced anodes for intermediate temperature SOFCs. In this respect nanocomposites offer great possibilities. Appropriate preparation procedures allow one to deposit nanodimensioned oxide particles, thus taking advantage of the reactivity of nanoclusters.[4] Moreover, an active oxide can be used as a support.

Cerium oxide and cobalt oxides can play an important role in oxidation reactions. Cerium oxide is a major component in the three-way catalysts (TWC) used for the treatment of automotive exhaust gases.[5] The oxygen storage capacity (OSC), associated with a fast Ce(IV)/Ce(III) redox process, is one of the key properties of this material. Moreover, cerium oxide is a mixed conductor exhibiting both ionic and electronic conductivity (n-type).[3] Co_3O_4 shows the highest catalytic activity for the combustion of carbon monoxide and of organic compounds and it may be included in formulation of catalyst for treatment of waste gases.[6] Moreover, cobalt oxides are used as catalyst in the hydrocracking process of crude fuels, in several oxidation reactions,[7,8] as well as in ammonia oxidation.[9,10]

Because of these reasons, as part of a comprehensive study concerning the reactivity of ceria-based nanocomposites, the present contribution focuses on the synthesis and characterization of cobalt oxide/ceria nanocomposite powder samples. A deeper investigation of the catalytic activity will be the subject of following papers. As a matter of fact, despite the promising behavior of cobalt oxides and ceria, only few papers concern the oxides containing cobalt and cerium; moreover, they are focused on mixed oxides obtained by coprecititation,[11] while nanocomposites could be an interesting choice.

* Corresponding author. Tel.: ++39-049-8275196. Fax: ++39-049-8275161. E-mail: antonella.glisenti@unipd.it.

(1) Carrette, L.; Friedrich, K. A.; Stimming, U. *ChemPhysChem* **2000**, *1*, 162.
(2) Larmine, J.; Dicks, A. In *Fuel Cell Systems Explained*; Wiley: New York, 2000.
(3) Minh, N. Q. and Takahashi, T. In *Science and Technology of Ceramic Fuel Cells*; Elsevier: New York, 1995.
(4) Klabunde, K. In *Nanoscale Materials in Chemistry*; Wiley-Interscience: New York, 2001.
(5) Trovarelli, A. *Catal. Rev. Sci. Eng.* **1996**, *38*, 439.
(6) Spivey, J. J. *Ind. Eng. Chem. Res.* **1987**, *26*, 2165.
(7) Natile, M. M.; Glisenti, A. *J. Mol. Catal. A, Chem.* **2004**, *217*, 175.
(8) Trimm, D. L. In *Design of Industrial Catalysts*, Elsevier: New York, 1980; Chapter 7.
(9) Chinchen, G.; Davies, P.; Sampson, R. J. In *The Historical Development of Catalytic Oxidation Processes in Catalysis: Science and Technology*; Anderson, J. R., Boudart, M., Eds.; Springer-Verlag: New York, 1987; Vol. 8, Chapter 1.
(10) Satterfeld, C. N. In *Heterogeneous Catalysis in Industrial Practice*, 2nd ed.; McGraw-Hill: New York, 1991; Chapter 8.

10.1021/cm048748u CCC: $30.25
Published on Web 05/25/2005

Several nanocomposite samples with increasing Co/Ce atomic ratio are obtained by wet impregnation and characterized by means of X-ray diffraction (XRD), thermal analysis (TGA), BET, as well as X-ray photoelectron (XPS), diffuse reflectance infrared Fourier transform (DRIFT), and inductively coupled plasma atomic emission (ICP-AES) spectroscopic techniques. The growing mechanism and the powder morphology are investigated by means of transmission electron microscopy (TEM) and energy dispersive spectroscopy (EDS). To get a more accurate characterization of the CoO_x/CeO_2 catalysts, the active sites distributed on the sample surfaces are investigated by means of probe molecules (pyridine and carbon dioxide)[12−19] and compared with those observed on CeO_2[20] and cobalt oxides.[21]

Finally, the interaction between the nanocomposites and methanol is considered: methanol is both an important probe molecule and an interesting combustible for fuel cells.[2]

Experimental Session

(a) Catalyst Preparation. The CeO_2 support was prepared by precipitation from an aqueous solution of $Ce(NO_3)_3 \cdot 6H_2O$ (Strem, 99.9%). The solution was obtained by dissolving the nitrate in distilled water and adding NH_4OH (Carlo Erba, water solution 30%) until pH = 10.

The precipitate was filtered out and washed with distilled water until pH = 7 and then it was dried at 373 K for 5 h and calcined at 523 K for 5 h. The supporting powder was investigated by means of XRD, XP, and DRIFT spectroscopic techniques and thermal analysis and was confirmed to be CeO_2 before the deposition procedure. The CoO_x/CeO_2 nanocomposite systems were obtained by wet impregnation of CeO_2 (heated at 523 K) with aqueous solutions containing increasing quantities of $Co(NO_3)_2 \cdot 6H_2O$ [Co/Ce nominal atomic ratio = 0.005, 0.010, 0.025, 0.040, 0.055, 0.075]. The obtained suspension was maintained under stirring for 2 days and then kept at rest for 1 day. Water was evaporated in air and the obtained solid was dried at 373 K for 5 h and at 1023 K for 5 h (in air).

(b) XPS Measurements. XPS spectra were recorded using a Perkin-Elmer PHI 5600 ci spectrometer with a standard Al Kα source (1486.6 eV) working at 350 W. The working pressure was less than 1×10^{-8} Pa. The spectrometer was calibrated by assuming the binding energy (BE) of the Au $4f_{7/2}$ line to lie at 84.0 eV with respect to the Fermi level. Extended spectra (survey) were collected in the range 0−1350 eV (187.85 eV pass energy, 0.4 eV step, 0.05 s $step^{-1}$). Detailed spectra were recorded for the following regions: C 1s, O 1s, Ce 3d, Ce 4d, and Co $2p_{3/2}$ (11.75 eV pass energy, 0.1 eV step, 0.1 s $step^{-1}$). The standard deviation in the BE values of the XPS line is 0.10 eV. The atomic percentage, after a Shirley-type background subtraction,[22] was evaluated using the PHI sensitivity factors.[23] To take into consideration charging problems, the C 1s peak at 285.0 eV was considered and the peaks BE differences were evaluated.

The sample for the XPS analysis was processed as a pellet by pressing the catalyst powder at ca. 7×10^6 Pa for 10 min; the pellet was then evacuated for 12 h at ca. 1×10^3 Pa.

(c) TEM and EDS. Transmission electron micrographs were obtained with a Philips JRM 2010 electron microscope using 200 kV primary voltage. The samples used for TEM observations were prepared by dispersing some products in ethanol followed by ultrasonic vibration for 30 min and then placing a drop of the dispersion onto a copper grid (200 Cu) coated with a layer of amorphous carbon. Energy dispersive spectroscopy (EDS) measurements were carried out by means of a LINK INCA 100 microanalysis system. The diameter of the analyzed spot was 5−15 nm.

(d) Thermal Analysis. Thermogravimetric analysis (TGA) was carried out in a controlled atmosphere using the Simultaneous Differential Techniques (SDT) 2960 of TA Instruments. Thermograms were recorded at 5 K min^{-1} heating rate in air and in nitrogen flow. The temperature ranged from room temperature (rt) to 1273 K.

(e) XRD Measurements. XRD patterns were obtained with a Bruker D8 Advance diffractometer with Bragg−Brentano geometry using Cu Kα radiation (40 kV, 40 mA, $\lambda = 0.154$ nm).

(f) BET Measurements. BET surface area measurements were determined using a Carlo Erba Sorptomatic 1900 adsorbing N_2 at its boiling temperature. The sample was previously evacuated for 6 h at 423 K.

(g) ICP-AES Measurements. The amounts of Co and Ce were determined by ICP-AES (ICP Spectro Flame Sops/N6410/95A) by using the method of standard additions and the following emission lines: $\lambda(Co) = 238.89$ nm and $\lambda(Ce) = 413.38$ nm. The argon reference line was set at 430.1 nm. The analytical determinations were performed on microwave-digested samples by means of a Millestone Ethos 1600 (2.45 GHz) microwave system. The mineralization of the powder was performed by treating 15−20 mg of the sample with 5 mL of a solution consisting of HNO_3 (Carlo Erba 69.5%) (25% vol) and HCl (Carlo Erba 37%) (75% vol) in a Teflon vessel at 250−650 W.

(h) DRIFT Measurements and Reaction Conditions. The IR spectra were collected in a Bruker IFS 66 spectrometer (accumulating 128 scans at a resolution of 4 cm^{-1}) and displayed in Kubelka−Munk units.[24,25] The temperature of the powder was checked by means of a thermocouple inserted into the sample holder directly in contact with the powder.

Prior to each experiment, ca. 50 mg of the sample was loaded in the sample cup of a low-temperature reaction chamber (CHC) installed in the Praying Mantis accessory for diffuse reflection spectroscopy (Harrick Scientific Corp.) and fitted with ZnSe windows; the powder was kept in nitrogen flow to eliminate water traces until a stable IR spectrum was obtained (ca. 2 h). Then, the sample was exposed to the reactive species at a flow rate of 100−150 cm^3 min^{-1} before measurement. The background spectrum of the surface before exposure to the reactive gas was measured for spectra correction. It is noteworthy observing that all the reactivity tests were carried out on the samples "as prepared", avoiding the activation procedure; the influence of the activation procedure will be the subject of further works.

The CHC chamber was filled with the pyridine or the alcohol vapors flowing nitrogen through a bubbler containing the liquid,

(11) Kang, M.; Song, M. W.; Lee C. H. *Appl. Catal. A* **2003**, *251*, 143.
(12) Parry, E. P. *J. Catal.* **1963**, *2*, 371.
(13) Little L. H. In *Infrared Spectra of Adsorbed Species*; Academic Press: San Diego, CA, 1966; Chapter 7.
(14) Nortier, P.; Fourre, P.; Mohammed Saad, A. B.; Saur, O.; Lavalley, J. C. *Appl. Catal.* **1990**, *61*, 141.
(15) Busca, G. *Catal. Today* **1998**, *41*, 191.
(16) Auroux, A.; Gervasini, A. *J. Phys. Chem.* **1990**, *94*, 6371.
(17) Rethwisch, D. G.; Dumesic, J. A. *Langmuir* **1986**, *1−2*, 73.
(18) Lavalley, J. C. *Trends Phys. Chem.* **1991**, *2*, 305.
(19) Martin, D.; Duprez, D. *J. Mol. Catal. A: Chem.* **1997**, *118*, 113.
(20) unpublished data.
(21) Natile, M. M., Glisenti, A. *Chem. Mater.* **2003**, *15*, 2502.
(22) Shirley, D. A. *Phys. Rev.* **1972**, *55*, 4709.
(23) Moulder, J. F.; Stickle, W. F.; Sobol, P. E.; Bomben, K. D. In *Handbook of X-ray Photoelectron Spectroscopy*; Chastain, J., Ed.; Physical Electronics: Eden Prairie, MN, 1992.
(24) Kubelka, P.; Munk, F. *Z. Tech. Phys.* **1931**, *12*, 593.
(25) Kortum, G. In *Reflectance Spectroscopy*; Springer: New York, 1969.

Table 1. Specific Surface Area, Pore Volume, and Pore Diameter Measured for the Nanocomposite Samples, for the Supporting Ceria, and for a Ceria Sample Treated at the Same Temperature (1023 K) as the Nanocomposites

sample	specific surface area (m^2/g)	pore volume (cm^3/g)	pore diameter (nm)
CeO_2 treated a 523 K	37.9	0.090	3−10
CeO_2 treated a 1023 K	11.4	0.042	3−20
CoO_x/CeO_2 (Co/Ce = 0.010)	15.3	0.047	9.0
CoO_x/CeO_2 (Co/Ce = 0.055)	21.4	0.058	7.4

whereas for CO_2 (Air Liquide, 99.998%) the gas outlet was directly connected to the reaction chamber. Pyridine and methanol used for the chemisorption were taken from a commercial source (Sigma-Aldrich, spectroscopic grade) and used without further purification.

Results and Discussion

(a) CoO_x/CeO_2 Characterization. The heat treatment at 1023 K causes the specific surface area of ceria to decrease from 37.9 to 11.4 m^2/g. The decrease of the surface area is lower when cobalt is present; consistently, the pore volume decrease is higher in pure ceria (Table 1). The higher surface area in the nanocomposites is due to the cobalt oxide nanoclusters deposition.[4] Moreover, the pore size distribution is very disordered and ranges from 3 to 10 nm in ceria treated at 523 K and from 3 to 20 nm in ceria treated at 1023 K. In the nanocomposites, in contrast, the pore size distribution is very narrow (Table 1).

The XP spectra obtained for the powder oxides are shown in Figures 1 and 2, whereas the peak positions are summarized in Table 2.

The Ce 3d peak positions (signals V, V″, U, U″, and U‴ in Figure 1) agree with the data obtained for CeO_2 (Table 2). The comparison with the Ce 3d peak observed for the supporting oxide (Figure 1) suggests the presence of Ce(III): the signal V′, characteristic of Ce(III), is well-evident.[26,27] Ce(III) can be due to the treatment at 1023 K or to the deposition of cobalt oxide. The shape of the Ce 3d peak obtained on a CeO_2 sample treated at 1023 K (for 5 h) confirms the contribution of the cobalt oxide deposition to ceria reduction; the slight narrowing of the signals in the "U region" could suggest a chemical and/or structural reordering phenomenon. The detailed investigation of the Ce 4d spectral region suggests a reduction phenomenon only interesting the outer monolayers. In fact, the Ce 4d peak shape (Figure 1) does not change as a consequence of the heat treatment or the cobalt oxide deposition.[28]

The Co $2p_{3/2}$ XP spectra of the CoO_x/CeO_2 nanocomposites are compared with the ones obtained for CoO and Co_3O_4[29] in Figure 2. The Co $2p_{3/2}$ peak position (781.1−781.2 eV) and the shake-up signal at 786.7−786.9 eV agree with the presence of Co(II).[30−32]

This behavior is particularly evident in the samples with a lower cobalt content. As the preparation procedure is the same for all the impregnated samples, the effect of CeO_2 in the stabilization of CoO must be considered. Significantly, both CoO and CeO_2 are characterized by a cubic structure. At higher Co/Ce nominal atomic ratio, in contrast, the decrease of the shake-up contribution suggests a Co_3O_4 presence.

The positions of the O 1s XP peak (Figure 2) in the CoO_x/CeO_2 samples (529.4−529.6 eV) agree with the expected value for oxygen in ceria (Table 2). The fitting procedure shows a contribution at higher BE (531.2−531.6 eV) attributed to the presence of hydroxyl groups.[33] The lower hydroxylation of the nanocomposites with respect to CeO_2, evidenced by the comparison of the corresponding O 1s XP spectra (Figure 2), could indicate the grafting of cobalt oxide to CeO_2 by condensation of OH groups.[34]

The XP atomic composition is reported as a function of the nominal one in Table 3. The obtained Co/Ce atomic ratios are always lower than the corresponding nominal values (calculated from the weighted quantities), suggesting the diffusion of cobalt inside CeO_2. To investigate this hypothesis, the powder composition was determined by means of ICP-AES. The obtained Co/Ce atomic ratios (Table 3) are very similar to the nominal values, thus confirming the cobalt diffusion.

Figure 3 shows the XRD patterns of the samples richer in cobalt, $[Co/Ce]_{nominal} = 0.055$ and 0.075, and of the supporting CeO_2. The XRD patterns of the CoO_x/CeO_2 samples and of the support coincide: no diffraction peaks due to crystalline CoO or Co_3O_4 are observed. This demonstrates that cobalt oxide exists as highly dispersed or amorphous surface species or the cobalt amount is low.[35,36] The average diameter of CoO_x/CeO_2 crystallites, evaluated by means of the Scherrer formula,[37] is about 22 nm, whereas for the supporting ceria the particles diameter is about 15 nm. This difference is due to the treatment at 1023 K.

(26) Park, P. W.; Ledford J. S. *Langmuir* **1996**, *12*, 1794.
(27) Rama Rao, M. V.; Shripathi T. *J. Electron Spectrosc. Relat. Phenom.* **1997**, *87*, 121.
(28) Escape depth is higher for Ce 4d than Ce 3d photoelectrons. Fadley, C. S. In *Electron Spectroscopy: Theory, Techniques and Applications;* Brundle, C. R., Baker A. D., Eds.; Academic Press: New York,1978; Chapter 1.
(29) The Co_3O_4 reference sample was obtained by precipitation from an aqueous solution of cobalt nitrate; the precipitate was dried at 573 K for 10 h and treated at 1023 K for 20 h. The XRD outcomes are consistent with the presence of the Co_3O_4 spinel structure and the DRIFT spectra clearly shows the signals attributed to the longitudinal vibrations (at 695−698 cm^{-1} and 610−613 cm^{-1}). Co 2p XP peak positions agree with the presence of Co_3O_4: the almost complete absence of the shake-up peaks characteristic of the Co(II) in CoO is even more indicative of this situation. Co(II) and Co(III) oxides can be differentiated in XPS using their different magnetic properties. In fact, the XP spectra of Co(II) high-spin compounds, such as CoO, are characterized by an intense shake-up satellite structure at ca. 787.0 and 804.0 eV. Unlike in Co(II) compounds, in the low-spin Co(III) compounds, the satellite structure is weak or missing. Co_3O_4, a mixed-valence oxide, shows a weak satellite structure symptomatic of shake-up from the minor Co(II) component. The CoO was prepared by heating Co_3O_4 under high vacuum conditions (at 743 K for 33 h); to avoid the formation of Co_3O_4 on the surface, the CoO sample powder was kept and characterized in ultrahigh vacuum. Finally, the O/Co XP atomic ratio is 1.4 in the sample Co_3O_4 and 1.0 in the CoO powder. See also: Natile, N. N.; Glisenti, A. *Chem. Mater.* **2002**, *14*, 3090.
(30) Oku, M.; Hirokawa, K. *J. Electron Spectrosc. Relat. Phenom.* **1976**, *8*, 475.
(31) Hassel, M.; Freund, H.-J. *Surf. Sci.* **1995**, *325*, 163.
(32) Schenck, C. V.; Dillard, J. G.; Murray, J. W. *J. Colloid Interface Sci.* **1983**, *95*, 398.
(33) McIntyre, N. S.; Chan, T. C. In *Practical Surface Analysis 1*, 2nd ed.; Briggs, D., Seah, M. P., Eds.; Wiley: Chichester, 1990; Chapter 10.
(34) Schwarz, J. A.; Contescu, C.; Contescu, A. *Chem. Rev.* **1995**, *95*, 477.
(35) Bigey, C.; Hilaire L.; Maire, G. *J. Catal.* **2001**, *198*, 208.

Table 2. XPS Peak Positions (Binding Energy, eV) Obtained for the CoO_x/CeO_2 Supported Oxide Samples and for the Pure Oxide

XPS peak		Co/Ce = 0.005	Co/Ce = 0.010	Co/Ce = 0.025	Co/Ce = 0.040	Co/Ce = 0.055	Co/Ce = 0.075	CeO_2 (523 K)	Co_3O_4[29]	CoO[29]
Co $2p_{3/2}$			781.2	781.2	781.1	781.1	781.1		780.3	781.0
shake-up Co $2p_{3/2}$			786.8	786.7	786.7	786.9	786.9			786.8
Ce $3d_{5/2}$	V	882.6	882.6	882.7	882.7	882.6	882.7	882.9		
	V′	885.6	885.6	885.7	885.7	885.5	885.6			
	V″	889.0	889.0	888.9	889.0	888.9	889.0	889.0		
	V‴	898.5	898.6	898.6	898.5	898.5	898.6	898.7		
Ce 3d3/2	U	901.0	901.1	901.0	901.0	901.0	901.1	900.8		
	U′	903.9	903.9	904.2	904.1	904.0.0	903.9			
	U″	907.4	907.4	907.5	907.5	907.5	907.4	907.4		
	U‴	916.8	916.8	916.9	916.9	916.8	916.9	916.8		
Ce 4d	A	108.4	108.5	108.6	108.5	108.4	108.5	108.7		
	B	111.9	111.8	111.8	111.8	111.8	112.0	112.1		
	X‴	121.6	121.6	121.6	121.5	121.6	121.7	121.7		
	W‴	124.9	124.9	124.9	124.9	124.9	125.0	124.9		
O 1s		529.4	529.5	529.4	529.5	529.4	529.4	529.6	530.3	530.3
		531.4	531.3	531.2	531.6	531.4	531.4	531.3	531.4	
									532.8	

Two impregnated oxides characterized by the nominal atomic ratios Co/Ce = 0.010 and 0.055 were selected for a more detailed investigation.

The TEM image of the CoO_x/CeO_2 nanocomposite with $[Co/Ce]_{nominal} = 0.010$ (Figure 4A) shows the cobalt oxide particles deposited on the cubic CeO_2. This is confirmed by the EDS analysis. In agreement with the results obtained by means of the Sherrer formula, the dimensions of the ceria particles are around 20−25 nm. The deposited cobalt oxide clusters range around 6.5 nm. Moreover, HRTEM suggests a good crystallinity of the cobalt oxide particles (Figure 4B). In the TEM images of the CoO_x/CeO_2 sample with $[Co/Ce]_{nominal} = 0.055$ (Figure 4C), the cobalt oxide particles are not visible anymore; the EDS Co/Ce atomic ratio shows, however, the homogeneous distribution of cobalt (Table 4).[36]

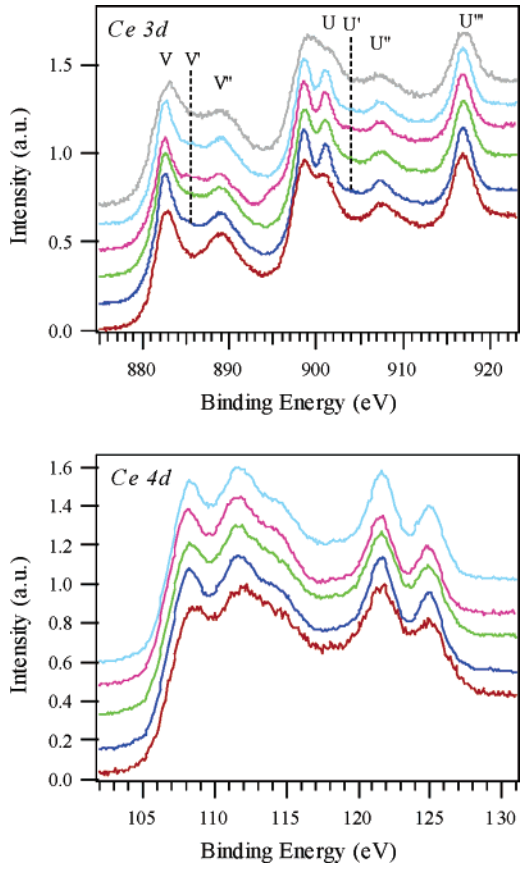

Figure 1. Ce 3d and Ce 4d XP spectra obtained on the CoO_x/CeO_2 supported oxides compared with the corresponding spectra of CeO_2: (red) CeO_2 treated at 523 K; (gray) CeO_2 treated at 1023 K; $[Co/Ce]_{nominal}$ = (blue) 0.010, (green) 0.025, (fuchsia) 0.055, (sky blue) 0.075. (The spectra are normalized with respect to their maximum value.)

TEM and EDS results suggest a complex growing mechanism: the formation of small cobalt oxide clusters is followed by their collapse to originate a homogeneous layer.[38]

The DRIFT spectra obtained for the samples with $[Co/Ce]_{nominal} = 0.010$ and 0.055 are reported, as a function of temperature, in Figures 5 and 6, respectively. At room temperature the presence of molecularly chemisorbed water is suggested by the corresponding bending (1627 cm^{-1}, see Figures 5b and 6b) and stretching (3692 cm^{-1} see Figures 5a and 6a) signals.[39−41] The broad band around 3400 cm^{-1} (Figures 5a and 6a) is due to H-bound hydroxyl groups.

At higher wavenumber the signals corresponding to bicoordinated hydroxyl groups (3632 and 3662 cm^{-1}) can be observed.[39] A lower hydroxylation of the nanocomposites with respect to the ceria heated at 1023 K is evident, despite the higher surface area (Figure 7). By comparing the DRIFT spectra of the nanocomposites with that of CeO_2 heated at 1023 K (Figure 7), it is evident that a significant part of the decrease of the hydroxyl groups can be attributed to the grafting mechanism. It is interesting to notice that the hydroxylation of the pure cobalt oxide is almost insignificant.[29]

The heat treatment causes the desorption of molecularly chemisorbed water molecules as well as the condensation of the H-bound hydroxyl groups (Figures 5a and 6a); at *T*

(36) As already observed, XRD patterns never show the contribution of cobalt oxide particles; commonly this is attributed to the small size of the crystallites, to the insufficient cobalt load, to the presence of strain factors and disorder, or to the low cobalt oxide content (see, as an example, Klug, H. P.; Alexander, L. E. *X-ray Diffraction Procedures—For Polycrystalline and Amorphous Materials*, 2nd ed.; Wiley: New York, 1974, Chapter 9). In this case, however, HRTEM data allow us to exclude the possibility of a disordered system.
(37) Enzo, S.; Polizzi, S.; Benedetti, A. *Z. Kristall.* **1985**, *170*, 275.
(38) Argile, C.; Rhead, G. E. *Surf. Sci. Rep.* **1989**, *10*, 277.
(39) Badri, A.; Binet C.; Lavalley, J.-C. *J. Chem. Soc., Faraday Trans.* **1996**, *92*, 4669.
(40) Binet, C.; Daturi, M.; Lavalley, J.-C. *Catal. Today* **1999**, *50*, 207.
(41) Daturi, M.; Finocchio, E.; Binet, C.; Lavalley, J.-C.; Fally, F.; Perrichon, V. *J. Phys. Chem. B* **1999**, *103*, 4884.

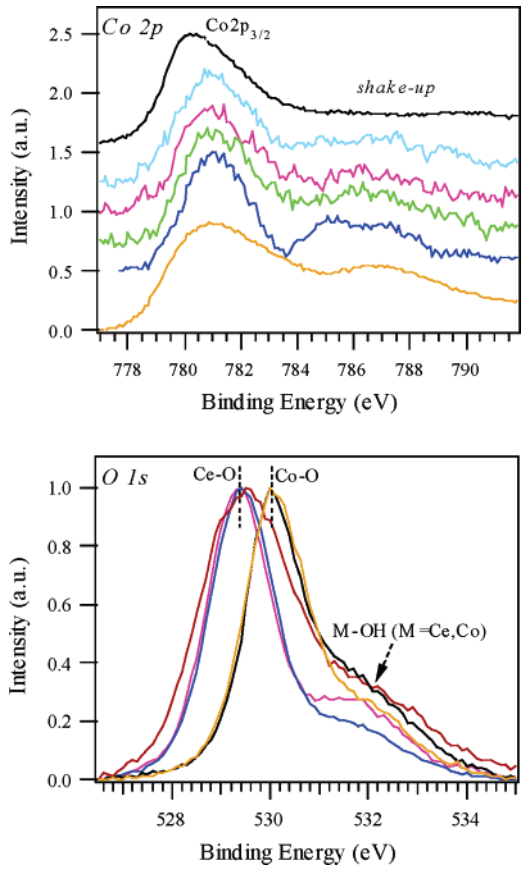

Figure 2. Co $2p_{3/2}$ and O 1s XP spectra obtained on the CoO_x/CeO_2 supported oxides compared with the corresponding spectra of CeO_2, CoO, and Co_3O_4: (red) CeO_2; (yellow) CoO; (black) Co_3O_4; $[Co/Ce]_{nominal}$ = (blue) 0.010, (green) 0.025 (fuchsia) 0.055, (sky blue) 0.075. (The spectra are normalized with respect to their maximum value.)

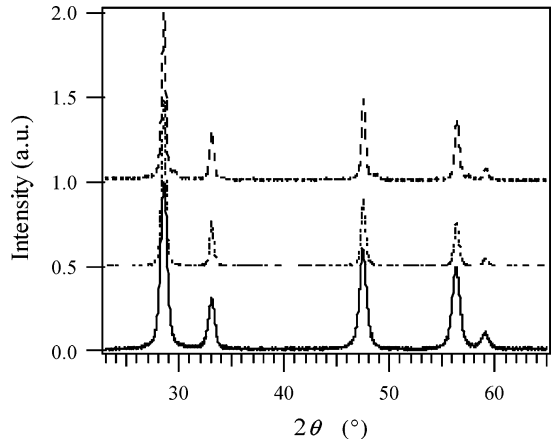

Figure 3. XRD patterns of CeO_2 (—) and of the CoO_x/CeO_2 supported oxides with $[Co/Ce]_{nominal}$ = (···) 0.055 and (---) 0.075.

Table 3. Nominal, XPS, and ICP-AES Atomic Composition of the Supported Oxides

sample	$[Co/Ce]_{nominal}$	$[Co\ 2p_{3/2}/Ce\ 3d]_{XPS}$	$[Co/Ce]_{ICP}$
1	0.005	0.001	0.0082
2	0.010	0.003	0.0125
3	0.025	0.020	0.0236
4	0.040	0.023	0.0394
5	0.055	0.024	0.0583
6	0.075	0.027	0.0699

≥ 373 K, the signals corresponding to these species are not visible anymore, whereas the contribution of tricoordinated hydroxyl groups becomes evident around 3500 cm^{-1}.[42−44]

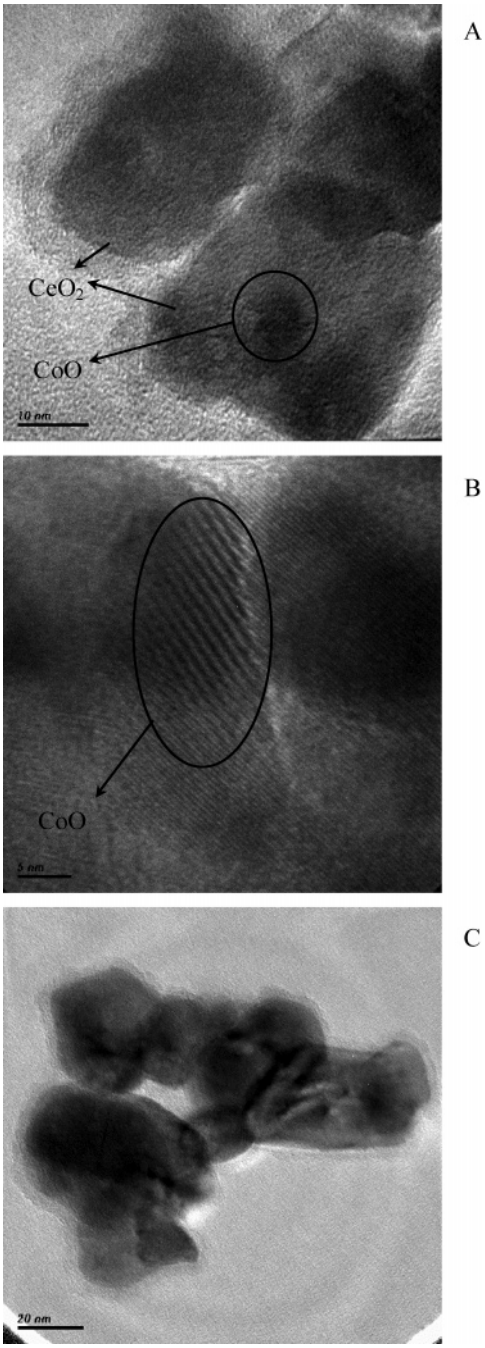

Figure 4. TEM (A) and HRTEM (B) images of the CoO_x/CeO_2 supported oxide with $[Co/Ce]_{nominal}$ = 0.010. TEM (C) image of the CoO_x/CeO_2 supported oxide with $[Co/Ce]_{nominal}$ = 0.055.

Table 4. EDS Atomic Ratios Obtained in Different Regions of the Supported Oxide with $[Co/Ce]_{nominal}$ = 0.055

region	Co/Ce	region	Co/Ce
1	0.026	3	0.024
2	0.023	4	0.020

The peaks due to bicoordinated OH groups shift toward lower wavenumber at increasing temperatures, suggesting a decrease of lateral interaction.[45]

(42) Laachir, A.; Perrichon, V.; Badri, A.; Lamotte, J.; Batherine, E.; Lavalley, J.-C.; El Fallah, J.; Hilaire, L.; LeNormand, F.; Quéméré, E.; Sauvion, G. N.; Touret, O. *J. Chem. Soc., Faraday Trans.* **1991**, *87*, 1601.
(43) Li, C.; Domen, K.; Maruya, K.; Onischi, T. *J. Catal.* **1990**, *125*, 445.
(44) Hara, M.; Kawamura, M.; Kondo, J. N.; Domen, K.; Maruya, K. *J. Phys. Chem.* **1996**, *100*, 14462.

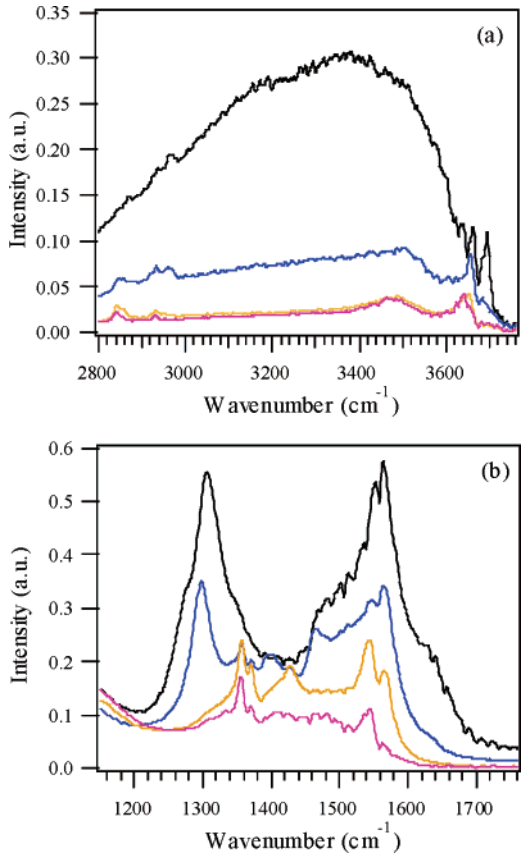

Figure 5. DRIFT spectra of the CoO_x/CeO_2 supported oxide with $[Co/Ce]_{nominal} = 0.010$ obtained at different temperatures: (black) rt, (blue) 373 K, (yellow) 473 K, and (fuchsia) 523 K. (a) Spectral region from 2800 to 3760 cm^{-1}; (b) spectral region from 1150 to 1760 cm^{-1}.

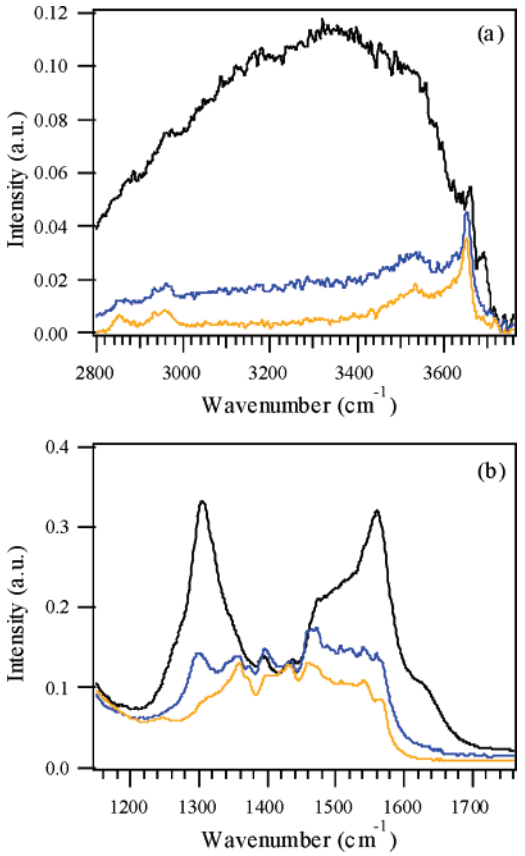

Figure 6. DRIFT spectra of the CoO_x/CeO_2 supported oxide with $[Co/Ce]_{nominal} = 0.055$ obtained at different temperatures: (black) rt, (blue) 373 K, and (yellow) 423 K. (a) Spectral region from 2800 to 3760 cm^{-1}; (b) spectral region from 1150 to 1760 cm^{-1}.

At $T \geq 373$ K, a weak signal at 3685 cm^{-1} is observed; this signal, already observed on reduced ceria,[20] is due to hydroxyl groups bicoordinated to Ce(III).[39,42]

In the IR spectral region characteristic of the O−C−O stretching vibrations, several signals can be observed (Figures 5b and 6b). The comparison with literature data suggests the presence of monodentate (1398 and 1470 cm^{-1}) and bidentate (1305 and 1560 cm^{-1}) carbonate species as well as inorganic carboxylates (shoulder at 1505 cm^{-1}).[40,46−48] The presence of these species is rather usual in ceria and ceria-based materials and has to be related to the interaction with atmospheric carbon dioxide.[49]

The heat treatment at rather low temperatures (373−473 K) causes the severe decrease of the signals attributed to carbonate species, suggesting a weak interaction between carbon dioxide and surface active sites. This behavior is particularly evident in the sample richer in cobalt and is probably a consequence of the cobalt oxide deposition; in fact, carbonate species are more difficult to eliminate from the surface of ceria,[20] whereas carbon dioxide was never observed to interact with Co_3O_4 surface.[21,29]

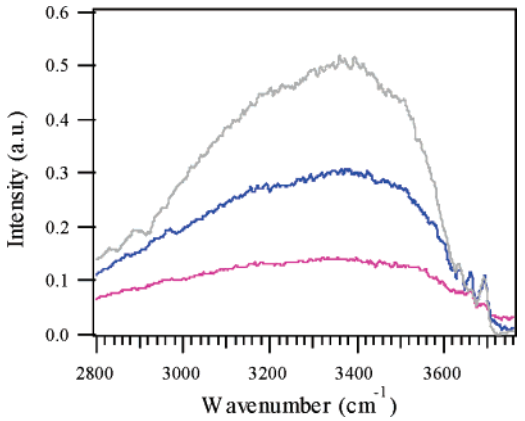

Figure 7. DRIFT spectra (obtained at rt) of the CoO_x/CeO_2 supported oxides with $[Co/Ce]_{nominal} = 0.010$ (blue) and 0.055 (fuchsia) compared with the corresponding spectra of CeO_2 treated at the same temperature of supported oxides (gray) at 1023 K: O−H stretching region.

The obtained results agree with the thermal analysis ones. Thermal analysis was carried out both in N_2 and in air flow without significant differences. Inspection of the thermal spectra recorded in N_2 indicates the desorption of water molecularly adsorbed on the surface at $T < 400$ K and the condensation of hydroxyl groups at higher temperatures (Figure 8). It is also evident that water loss is lower in the nanocomposites, despite the higher surface area, than ceria heated at the same temperature; this phenomenon is particularly marked in the sample characterized by a higher Co/Ce nominal atomic ratio. Consistently, water loss is very low

(45) Zecchina, A.; Lamberti, C.; Bordiga, S. *Catal. Today* **1998**, *41*, 169.
(46) Li, C.; Sakata Y.; Arai, T.; Domen, K.; Maruya, K.-I.; Onishi, T. *J. Chem. Soc., Faraday Trans. 1* **1989**, *85*, 4, 929.
(47) Li, C.; Sakata Y.; Arai, T.; Domen, K.; Maruya, K.-I.; Onishi, T. *J. Chem. Soc., Faraday Trans. 1* **1989**, *85*, 6, 1451.
(48) Gatehouse, B. M.; Livingstone S. E.; Nyholm, R. S. *J. Chem. Soc.* **1958**, 3137.
(49) Rosynek, M. P.; Magnuson, D. T. *J. Catal.* **1977**, *48*, 417.

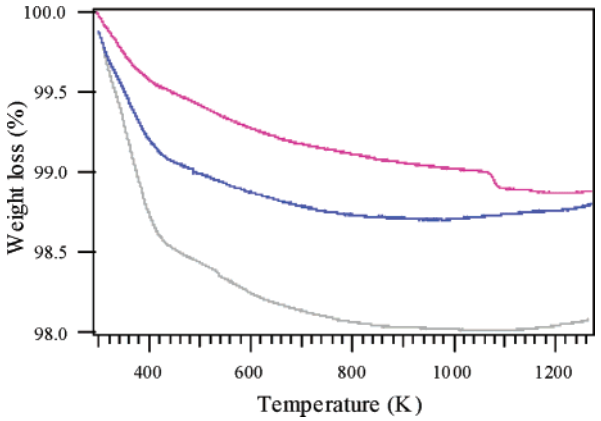

Figure 8. TGA spectra (recorded in N_2) of (gray) CeO_2 heated at 1023 K and of the supported oxide catalysts: $[Co/Ce]_{nominal}$ = (blue) 0.010, (fuchsia) 0.055.

in Co_3O_4.[29] Consequently, the lower hydroxylation shown by the nanocomposite surfaces (clearly suggested by IR and thermal analysis) cannot be attributed to the changes in surface area brought about by impregnation. The weight loss due to decomposition of carbonate species cannot be excluded.

The weight loss observed at about 1080 K in the sample with $[Co/Ce]_{nominal} = 0.055$ is due to the decomposition of Co_3O_4 to CoO (the decomposition occurs in air around 1200 K). It is noteworthy observing that a polycrystalline Co_3O_4 powder decomposes at lower temperature (in N_2 at 1033 K and in air at 1181 K), which suggests thus a stabilizing effect of the support.[21,29] Thermal analysis confirms the XPS results: in the nanocomposites with lower Co/Ce atomic ratio, Co(II) is prevalent, whereas Co_3O_4 is more evident with increasing cobalt content.

(b) CoO_x/CeO_2: Reaction with Pyridine and with CO_2. The DRIFT spectra obtained after exposure at room temperature of the supported oxide samples characterized by $[Co/Ce]_{nominal} = 0.010$ and 0.055 to pyridine are shown in Figures 9 and 10. The spectra inspection allows us to individuate several contributions at 1439, 1597 cm^{-1}, and from 1600 to 1700 cm^{-1}. The comparison with literature data suggests the presence of pyridine H-bound to the surface hydroxyl groups (1439 and 1597 cm^{-1}).[50−52] The peaks at higher wavenumber are attributed to pyridine interacting with acidic sites. In the sample with $[Co/Ce]_{nominal} = 0.010$ several contributions (1610, 1617, and 1634 cm^{-1}) agree with pyridine interacting with Lewis acidic sites[50,51] (Figure 9a). In the nanocomposite richer in cobalt only a peak (at 1617 cm^{-1}) is observed (Figure 10a). Consistently, when studying the interaction of pyridine with a Co_3O_4 surface, we observed that this oxide weakly interacts with pyridine.[21]

The intensity of the IR spectra obtained after exposing the nanocomposites to pyridine is significantly different, suggesting a higher amount of acidic sites on the surface of the sample with lower cobalt content.

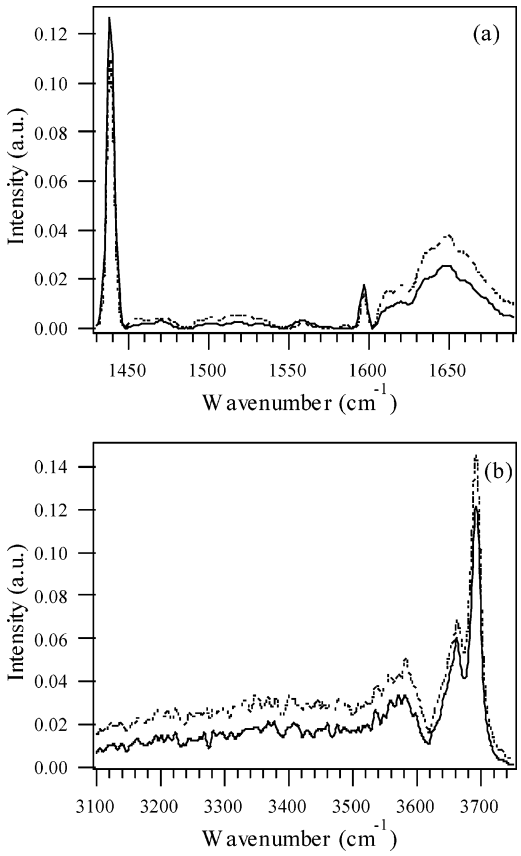

Figure 9. DRIFT spectra obtained after exposing the CoO_x/CeO_2 supported oxide with $[Co/Ce]_{nominal} = 0.010$ to pyridine (—) and successively to N_2 (···) at rt. (a) Spectral region from 1430 to 1690 cm^{-1}; (b) spectral region from 3100 to 3750 cm^{-1}.

The signal at 1647 cm^{-1} recorded for both samples is in agreement with the presence of oxidation species (α-pyridone, as an example, was observed to range from 1650 to 1680 cm^{-1} by Zaki et al.[50]). However, traces of Brønsted acidic sites cannot be ruled out.

New peaks appearing in the spectral region characteristic of the O−H stretching vibrations as a consequence of the exposure to pyridine (Figures 9b and 10b) suggest the perturbation of the hydroxyl groups. This result is particularly evident in the sample with $[Co/Ce]_{nominal} = 0.010$: the comparison with literature data indicates the attribution of the new signals to tricoordinated (3573 cm^{-1}), bicoordinated (3663 cm^{-1}), and monocoordinated (3691 cm^{-1}) hydroxyl.[39]

The evacuation with N_2 causes the desorption of liquidlike and H-bound pyridine, whereas pyridine interacting with acidic sites increases with exposure time, suggesting that the interaction of pyridine and the nanocomposite surfaces is a slow process.

The results obtained after exposing ceria and cobalt oxide to pyridine suggest that new acidic sites form as a consequence of the deposition of cobalt oxide on the ceria surface. As a matter of fact, pyridine interacts essentially by H-bound with hydroxyl groups on the supporting CeO_2 surface[20] and only rather weak Lewis acidic sites are observed on the Co_3O_4.[21]

At room temperature, CO_2 interacts with the CoO_x/CeO_2 samples, forming several carbonate species (Figure 11). The

(50) Zaki, M. I.; Hasan M. A.; Al-Sagheer, F. A.; Pasupulety, L. *Colloids Surf.* A **2001**, *190*, 261.
(51) Zaki, M. I.; Hussein G. A. M.; Mansour, S. A. A.; El-Ammawy, H. A. *J. Mol. Catal.* **1989**, *51*, 209.
(52) Zaki, M. I.; Hussein G. A. M.; Mansour, S. A. A.; Ismail, H. M.; Mekhemer, G. A. H. *Colloids Surf. A* **1997**, *127*, 47.

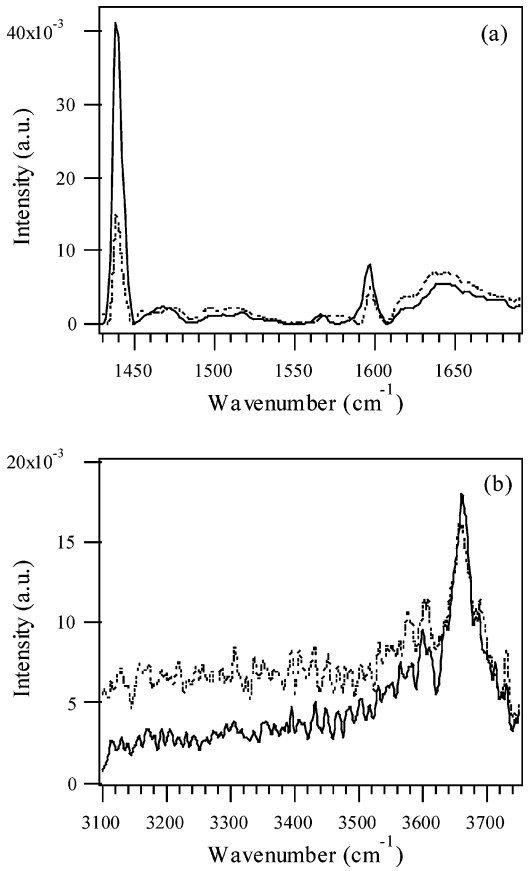

Figure 10. DRIFT spectra obtained after exposing the CoO_x/CeO_2 supported oxide with $[Co/Ce]_{nominal} = 0.055$ to pyridine (—) and successively to N_2 (···) at rt. (a) Spectral region from 1430 to 1690 cm^{-1}; (b) spectral region from 3100 to 3750 cm^{-1}.

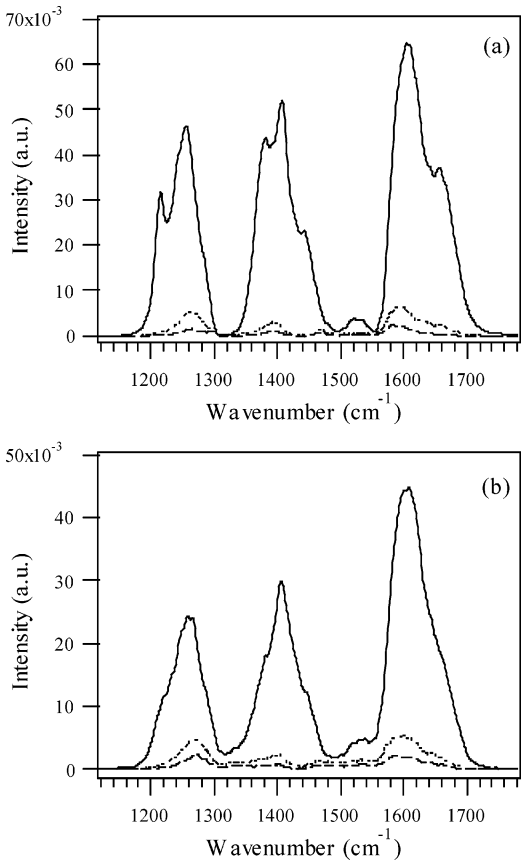

Figure 11. DRIFT spectra obtained at rt after exposing the CoO_x/CeO_2 supported oxides characterized by $[Co/Ce]_{nominal}$ = (a) 0.010 and (b) 0.055 to (—) CO_2 and successively to N_2 for (···) 3 min and (---) 15 min. Spectral region from 1120 to 1780 cm^{-1}.

signals observed in the sample characterized by $[Co/Ce]_{nominal} = 0.010$ (Figure 11a) agree with the formation of monodentate (1408 and 1441 cm^{-1}) and bidentate (1215, 1255, 1381 and 1605 cm^{-1}) carbonate species, bicarbonates[46,48] (1657 cm^{-1}), and inorganic carboxylates (1527 cm^{-1}). Similar results were obtained in the sample with $[Co/Ce]_{nominal} = 0.055$ (1260, 1381, 1407, 1446, 1520, and 1666 cm^{-1}; see Figure 11b). This means the presence of basic active sites and of complex sites constituted by a Lewis acidic site and a coordinatively unsaturated neighboring oxygen anion.

N_2 removes almost completely these species, suggesting a very weak interaction.

The comparison of the spectra obtained after the exposing to CO_2 shows that the formation of carbonate species is less evident in the sample richer in cobalt. It is interesting to note that Kang et al.[11] observed an activity decay in CO oxidation catalyzed by mixed oxides, obtained by coprecipitation, containing cobalt and cerium, and they attributed this decay to the carbon dioxide retention. It is important to note that cobalt oxide was not observed to interact with CO_2.[21]

(c) Interaction with Methanol. The extended IR spectra obtained after exposing the nanocomposites with $[Co/Ce]_{nominal} = 0.010$ and 0.055 to methanol and successively to N_2 at temperatures from room temperature to 573 K are shown in Figure 12. Several contributions are evident in the C−O stretching region of the two samples: 1034, 1052, and 1104 cm^{-1}. The signal at 1034 cm^{-1} is due to molecularly chemisorbed methanol, as confirmed by the corresponding symmetric and asymmetric C−H stretching contributions at 2837 and 2940 cm^{-1} (Figure 12a,b).[53,54] The comparison with literature data[40,43,55−58] suggests the formation of methoxy species monocoordinated (1104 cm^{-1}) and bicoordinated (1052 cm^{-1}) to Ce(IV). This result is confirmed by the signals corresponding to the symmetric and asymmetric C−H stretching observed at 2805, 2910, and 2922 cm^{-1}.[55,56]

Direct dissociation is preferred, as suggested by the signal at 3662 cm^{-1} attributed to bicoordinated hydroxyl groups (Figure 12). The position of this signal is almost identical to that observed on the sample before the exposure to methanol. Methanol dissociation is more evident in the nanocomposite with lower cobalt content, as evidenced by the comparison of the corresponding IR spectra (Figure 12a,b). This result is consistent with the differences in the acidic sites distribution observed in the samples with $[Co/Ce]_{nominal} = 0.010$ and 0.055. The higher wavenumber contribution around 3692 cm^{-1} observed on both the samples suggests also a condensation mechanism between methanol

(53) Falk, M.; Whalley, E. *J. Chem. Phys.* **1961**, *34*, 1554.
(54) Herzberg, G. In *Infrared and Raman Spectra of Polyatomic Molecules;* Van Nostrand: New York, 1949.
(55) Badri, A.; Binet C.; Lavalley, J.-C. *J. Chem. Soc., Faraday Trans.* **1997**, *93*, 1159.
(56) Siokou, A.; Nix, R. M. *J. Phys. Chem. B* **1999**, *103*, 6984.
(57) Binet, C.; Daturi M. *Catal. Today* **2001**, *70*, 155
(58) Binet, C.; Jadi, A.; Lavalley, J.-C. *J. Chim. Phys.* **1992**, *89*, 1441.

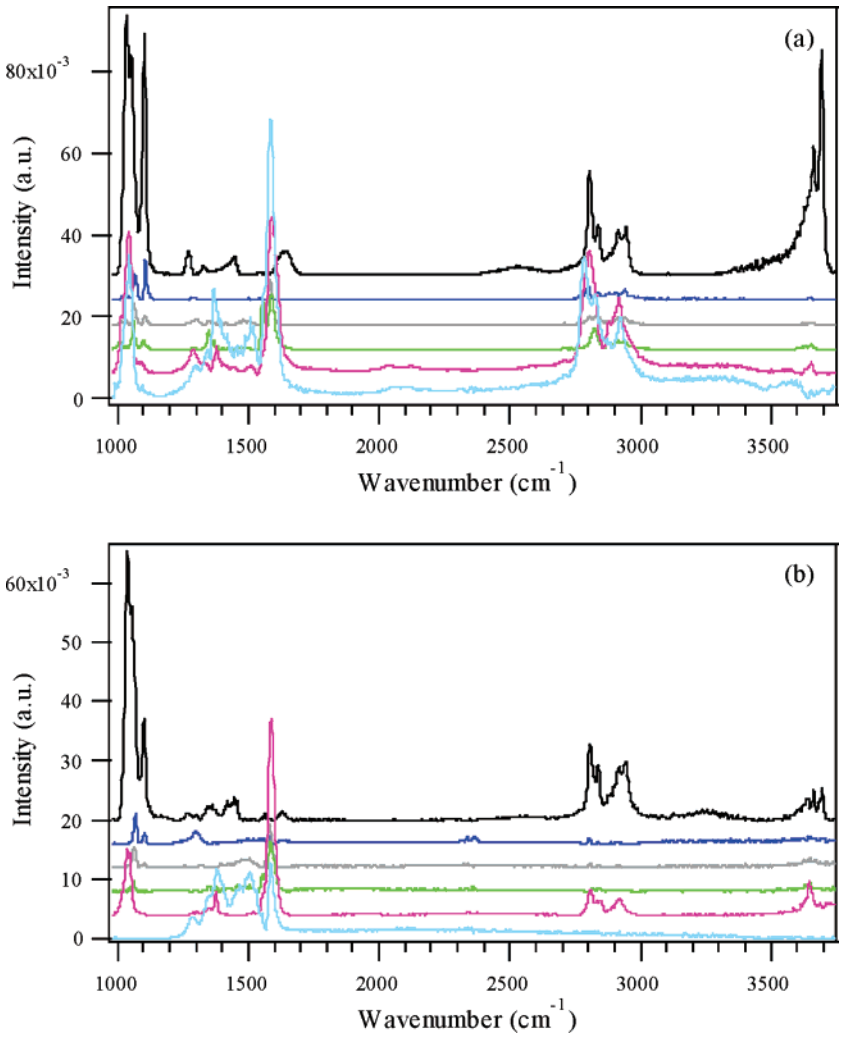

Figure 12. DRIFT spectra obtained after exposing the CoO_x/CeO_2 supported oxides with $[Co/Ce]_{nominal}$ = (a) 0.010 and (b) 0.055 to methanol + N_2 and successively to N_2 at different temperatures: (black) rt, (blue) 373 K, (gray) 403 K, (green) 433 K, (fuchsia) 523 K, and (sky blue) 573 K. Spectral region from 980 to 3740 cm^{-1}.

and hydroxyl groups. The formation of water is also confirmed by the corresponding OH bending peak at 1630 cm^{-1}. The lower wavenumber tail around 3400−3500 cm^{-1} observed for the sample with $[Co/Ce]_{nominal} = 0.010$ is due to H-bound hydroxyl groups.

Weak signals at 1273 and 1448 cm^{-1} (Figure 12) suggest the formation of carbonate species and thus a certain oxidizing capability at room temperature; this phenomenon is more evident in the sample with lower Co/Ce atomic ratio (Figure 12a).

At higher temperature, the contributions attributed to molecularly chemisorbed methanol (at 1034 cm^{-1}) and to the different methoxy groups (at 1052 and 1104 cm^{-1}) are not anymore revealed: only two intense signals are evident at 1066 and 1090−1095 cm^{-1}. To understand this result, several points have to be considered. First, bicoordinated methoxy groups are usually more stable than monocoordinated ones at high temperatures; moreover, the C−O stretching frequencies shift toward higher wavenumber on reduced ceria. Consistently, both the conversion of monocoordinated into the bicoordinated methoxy species and the formation of bicoordinated methoxy groups on the reduced surface of ceria can explain the observed results.[59]

At 523 K, new intense contributions can be observed in the C−O and C−H stretching regions (1018, 1040, 2805, and 2917 cm^{-1}), suggesting the formation of methoxy groups three-coordinated to Ce(III) and Ce(IV).[55,56] A similar behavior was observed in the supporting ceria.[20]

In the sample with lower cobalt content, formates (1350, 1559, and 1589 cm^{-1})[43,56] and inorganic carboxylates (1299 and 1508 cm^{-1})[47] form after exposure at 403 K (Figure 13a). At $T \geq 433$ K, the intensity of the signals attributed to formate increases and the presence of new peaks at 1368 and 1381 cm^{-1} suggests the presence of a different bidentate formate. Consistently with the increment of formate species, the contributions due to the methoxy groups decrease. In the sample with $[Co/Ce]_{nominal} = 0.055$ mono- and bicoordinated formate species (signals at 1350, 1379, 1553, and

(59) The C−O stretching frequency of monocoordinated methoxy groups ranges around 1105−1108 cm^{-1} and shifts around 1117 cm^{-1} in reduced ceria; the C−O stretching frequency of bicoordinated methoxy groups ranges around 1042−1065 cm^{-1} and shifts at about 1067−1087 cm^{-1} in reduced ceria; (see also refs 55−58). The peaks at 1066 cm^{-1} and about 1090−1095 cm^{-1} may be the result of the shift toward higher frequencies of the bicoordinated OH groups consequent to the reduction of ceria and of the shift toward lower wavenumbers due to the conversion of mono-coordinate into bi-coordinated methoxy groups.

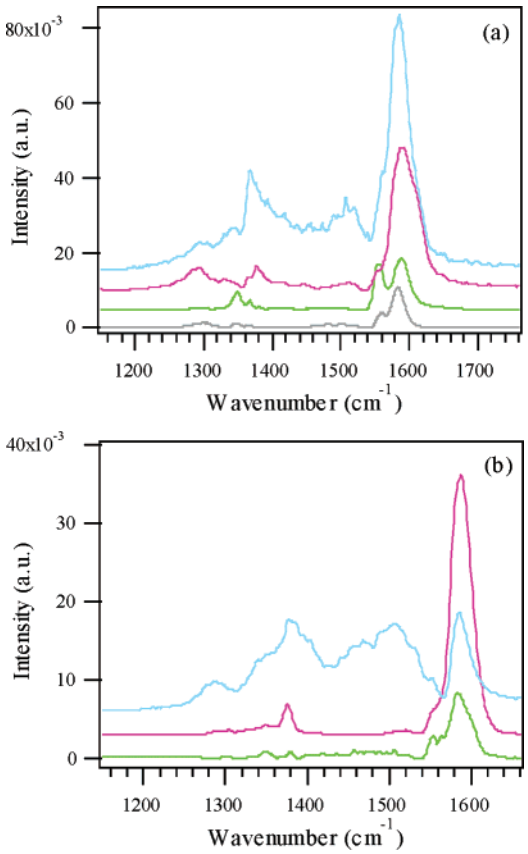

Figure 13. DRIFT spectra obtained after exposing the CoO_x/CeO_2 supported oxides with $[Co/Ce]_{nominal}$ = (a) 0.010 and (b) 0.055 to methanol + N_2 and successively to N_2 at different temperatures: (gray) 403 K, (green) 433 K, (fuchsia) 523 K, and (sky blue) 573 K. Spectral region from 1150 to 1760 cm^{-1}.

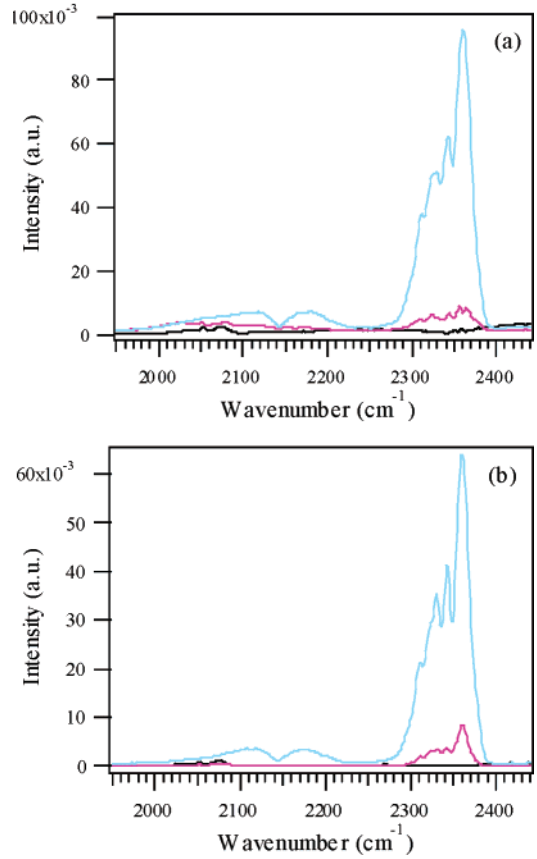

Figure 14. DRIFT spectra obtained after exposing the CoO_x/CeO_2 supported oxides with $[Co/Ce]_{nominal}$ = (a) 0.010 and (b) 0.055 to methanol + N_2 at different temperatures: (black) rt, (fuchsia) 523 K, and (sky blue) 573 K. Spectral region from 1950 to 2440 cm^{-1}.

1583 cm^{-1}) are evident at $T \geq 433$ K, whereas inorganic carboxylates form at 573 K (Figure 13b).

At 523 K, several signals (2310, 2322, 2344, and 2357 cm^{-1}) suggest on both the samples the formation of carbon dioxide. At 573 K, CO (2111 and 2176 cm^{-1}) is also evident (Figure 14). The formation of carbon dioxide increases with temperature.

The comparison between the spectra obtained after exposing the samples with $[Co/Ce]_{nominal}$ = 0.010 and 0.055 to methanol at 573 K (Figure 15) indicates that (1) the oxidation of methanol is more effective in the sample with $[Co/Ce]_{nominal}$ = 0.055; (2) in the sample with lower cobalt content, formates are more difficult to remove from the catalyst surface; this last assert is in accordance with the more evident acidic/basic character observed.

(d) Interaction with Methanol and Water. The sample with $[Co/Ce]_{nominal}$ = 0.055 was exposed to a water + methanol mixture and the obtained spectra are shown in Figure 16. The presence of water in the reactive mixture does not modify the capability of the catalyst to dissociate methanol. The signals observed after exposure at room temperature agree with the presence of monocoordinated (1104 cm^{-1}) and bicoordinated (1052 and 1060 cm^{-1}) methoxy groups and hydroxyl groups (3662 cm^{-1}) and molecularly chemisorbed water (3690 cm^{-1}). At 523 K, new methoxy species evidenced by signals at 1020 and 1038 cm^{-1} are consistent with the formation of new active sites for the dissociation reaction.

The temperature of oxidation to formate species (contributions at 1290, 1353, 1375, 1558, and 1585 cm^{-1}) is lower in the presence of water (373 K instead of 433 K). It is noteworthy observing that the formation of intermediate oxidation products (i.e. carbon monoxide) is not evident if water is present. The mechanism of the water−gas shift reaction and the role of ceria in this reaction are not completely clear. At least two mechanisms have been hypothesized: one is a redox process involving the interaction of adsorbed CO with ceria to form carbon dioxide, whereas the surface oxygen vacancy is saturated by oxygen from water.[60−63] Another mechanism suggests the formation of surface formates as a consequence of the interaction between carbon monoxide and the hydroxyl groups distributed on the ceria surface.[64−70] The last mechanism was also considered in methanol decomposition;

(60) Bunleisin, T.; Gorte, R.; Graham, G. *Appl. Catal. B* **1998**, *15*, 107.
(61) Hilaire, S.; Wang, X.; Luo, T.; Gorte, R. J.; Wagner, J. *Appl. Catal.* **2001**, *215*, 271.
(62) Li, Y.; Fu, Q.; Flytzani-Stephanopoulos, M. *Appl. Catal.* B **2000**, *27*, 179.
(63) Fu, Q.; Weber, A.; Flytzani-Stephanopoulos, M. *Catal. Lett.* **2001**, *77*, 87.
(64) Shido, T.; Iwasawa, Y. *J. Catal.* **1993**, *141*, 71.
(65) Shido, T.; Iwasawa, Y. *J. Catal.* **1992**, *136*, 493.
(66) Lavalley, J. C. *Catal. Today* **1996**, *27*, 377.
(67) Shido, T.; Iwasawa, Y. *J. Catal.* **1991**, *129*, 343.
(68) Shido, T.; Asakura, K.; Iwasawa, Y. *J. Catal.* **1990**, *122*, 55.
(69) Yamashita, K.; Naito, S.; Tamaru, K. *J. Catal.* **1985**, *94*, 353.
(70) Jacobs, G.; Patterson, P. M.; Williams, L. Sparks, D.; Davis, B. H. *Catal. Lett.* **2004**, *96*, 97.

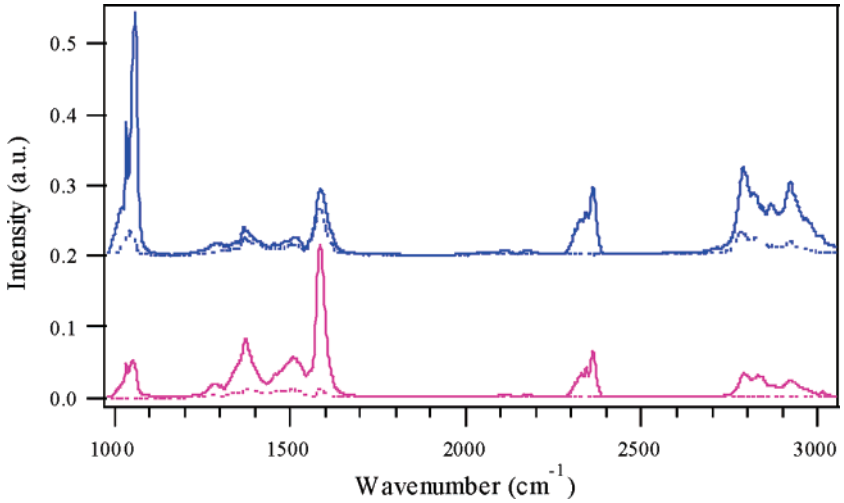

Figure 15. DRIFT spectra obtained after exposing (at 573 K) the CoO_x/CeO_2 supported oxides with $[Co/Ce]_{nominal} = 0.010$ (blue) and 0.055 (fuchsia) to methanol + N_2 (continuous line) and successively to N_2 (dotted line). Spectral region from 980 to 3050 cm^{-1}.

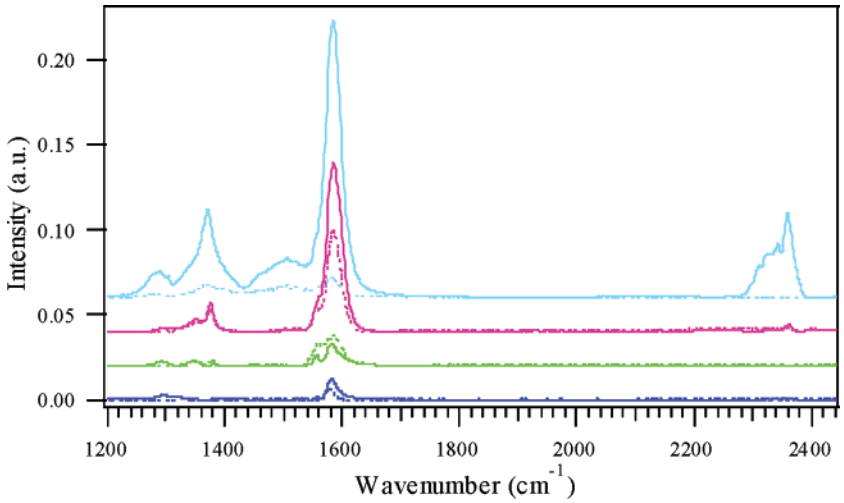

Figure 16. DRIFT spectra obtained after exposing the CoO_x/CeO_2 supported oxide with $[Co/Ce]_{nominal} = 0.055$ to methanol + H_2O + N_2 (continuous line) and successively to N_2 (dotted line) at different temperatures: (blue) 373 K, (green) 423 K, (fuchsia) 523 K, and (sky blue) 573 K. Spectral region from 1200 to 2440 cm^{-1}.

moreover, it seems not to disagree with the results presented in this paper.

At 573 K, nitrogen completely removes all the reaction products from the supported oxide surface.

Conclusions

In this paper CoO_x/CeO_2 nanocomposite samples with different Co/Ce atomic ratios (Co/Ce nominal atomic ratio = 0.005, 0.010, 0.025, 0.040, 0.055, 0.075) were synthesized by wet impregnation and characterized by means of XRD, TGA, BET, XP, DRIFT, and ICP-AE spectroscopic techniques as well as with TEM and EDS. The active sites distributed on the sample surfaces were also investigated by studying the interaction with probe molecules (pyridine and CO_2).

XRD pattern are consistent with the presence of cubic CeO_2, whereas the contributions due to cobalt oxide were never observed. The mean diameter of the CoO_x/CeO_2 particles ranges around 22 nm.

Nanocomposites show a lower specific surface area than the supporting CeO_2 heated at 523 K, but higher than the one treated at 1023 K.

XPS data are consistent with the prevalent presence of CoO in sample with low cobalt content, whereas Co_3O_4 is well-evident in the sample characterized by higher Co/Ce atomic ratios.

Ce(III) forms on the surface of ceria as a consequence of the heat treatment and the cobalt oxide deposition.

TEM images of nanocomposites at low cobalt content ($[Co/Ce]_{nominal} = 0.010$) suggest the deposition of 2D cobalt oxide clusters (diameter = 6.5 nm) on the ceria surface. With increasing cobalt content the cobalt oxide is homogeneously distributed (as indicated by TEM and EDS results) on the CeO_2 surface.

The exposure to pyridine suggests the presence of three Lewis acidic sites on the nanocomposite with $[Co/Ce]_{nominal} = 0.010$ and of a single Lewis acidic site on the sample with $[Co/Ce]_{nominal} = 0.055$; the presence of oxidation species is evident independently of the cobalt content.

The exposure to CO_2 allows us to recognize the presence of basic sites and of complex sites constituted by a Lewis acidic site and a coordinatively unsaturated neighboring oxygen anion. Basic and complex sites are less evident with increasing Co/Ce atomic ratio.

Methanol interacts both molecularly and dissociatively with the CoO_x/CeO_2 samples; the dissociation is prevalent in the nanocomposites characterized by a lower cobalt content.

The oxidation of methanol to formate species and inorganic carboxylates is evident at rather low temperatures (403 K with $[Co/Ce]_{nominal} = 0.010$ and 433 K with $[Co/Ce]_{nominal} = 0.055$). At 523 K the formation of carbon monoxide and carbon dioxide is evident.

When water is added to methanol, the oxidation temperature decreases to 373 K and the formation of carbon monoxide is not observed.

Acknowledgment. The authors gratefully acknowledge Prof. E. Tondello for helpful discussions, Dr. R. Saini for thermal analysis, Prof. L. Storaro for the BET measurements, Dr. G. Zanmarchi for the ICP-AES analyses, and INSTM for financial support.

CM048748U